

FILE COPY  
NO. 2-W

N 62 506-0

# NATIONAL ADVISORY COMMITTEE FOR AERONAUTICS

REPORT No. 680

## THE EFFECT OF NACELLE-PROPELLER DIAMETER RATIO ON BODY INTERFERENCE AND ON PROPELLER AND COOLING CHARACTERISTICS

By JAMES G. McHUGH and ELDRIDGE H. DERRING



# CASE FILE COPY

1939

FILE COPY

To be returned to  
the files of the National  
Advisory Committee  
for Aeronautics  
Washington, D. C.

## AERONAUTIC SYMBOLS

### I. FUNDAMENTAL AND DERIVED UNITS

	Symbol	Metric		English	
		Unit	Abbreviation	Unit	Abbreviation
Length-----	<i>l</i>	meter-----	m	foot (or mile)-----	ft. (or mi.)
Time-----	<i>t</i>	second-----	s	second (or hour)-----	sec. (or hr.)
Force-----	<i>F</i>	weight of 1 kilogram-----	kg	weight of 1 pound-----	lb.
Power-----	<i>P</i>	horsepower (metric)-----	k.p.h.	horsepower-----	hp.
Speed-----	<i>V</i>	{kilometers per hour----- meters per second-----}	m.p.s.	miles per hour----- feet per second-----	m.p.h. f.p.s.

### 2. GENERAL SYMBOLS

- $W$ , Weight =  $mg$   
 $g$ , Standard acceleration of gravity = 9.80665  
 m/s<sup>2</sup> or 32.1740 ft./sec.<sup>2</sup>  
 $m$ , Mass =  $\frac{W}{g}$   
 $I$ , Moment of inertia =  $mk^2$ . (Indicate axis of radius of gyration  $k$  by proper subscript.)  
 $\mu$ , Coefficient of viscosity

- $\nu$ , Kinematic viscosity  
 $\rho$ , Density (mass per unit volume)  
 Standard density of dry air, 0.12497 kg·m<sup>-3</sup>·s<sup>2</sup> at 15° C. and 760 mm; or 0.002378 lb.-ft.<sup>-4</sup> sec.<sup>2</sup>  
 Specific weight of "standard" air, 1.2255 kg/m<sup>3</sup> or 0.07651 lb./cu. ft.

### 3. AERODYNAMIC SYMBOLS

- $S$ , Area  
 $S_w$ , Area of wing  
 $G$ , Gap  
 $b$ , Span  
 $c$ , Chord  
 $b^2$   
 $\bar{S}$ , Aspect ratio  
 $V$ , True air speed  
 $q$ , Dynamic pressure =  $\frac{1}{2}\rho V^2$   
 $L$ , Lift, absolute coefficient  $C_L = \frac{L}{qS}$   
 $D$ , Drag, absolute coefficient  $C_D = \frac{D}{qS}$   
 $D_0$ , Profile drag, absolute coefficient  $C_{D_0} = \frac{D_0}{qS}$   
 $D_t$ , Induced drag, absolute coefficient  $C_{D_t} = \frac{D_t}{qS}$   
 $D_p$ , Parasite drag, absolute coefficient  $C_{D_p} = \frac{D_p}{qS}$   
 $C$ , Cross-wind force, absolute coefficient  $C_c = \frac{C}{qS}$   
 $R$ , Resultant force

- $i_w$ , Angle of setting of wings (relative to thrust line)  
 $i_t$ , Angle of stabilizer setting (relative to thrust line)  
 $Q$ , Resultant moment  
 $\Omega$ , Resultant angular velocity  
 $\rho \frac{Vl}{\mu}$ , Reynolds Number, where  $l$  is a linear dimension (e.g., for a model airfoil 3 in. chord, 100 m.p.h. normal pressure at 15° C., the corresponding number is 234,000; or for a model of 10 cm chord, 40 m.p.s., the corresponding number is 274,000)  
 $C_p$ , Center-of-pressure coefficient (ratio of distance of c.p. from leading edge to chord length)  
 $\alpha$ , Angle of attack  
 $\epsilon$ , Angle of downwash  
 $\alpha_0$ , Angle of attack, infinite aspect ratio  
 $\alpha_t$ , Angle of attack, induced  
 $\alpha_a$ , Angle of attack, absolute (measured from zero-lift position)  
 $\gamma$ , Flight-path angle

---

---

## **REPORT No. 680**

---

### **THE EFFECT OF NACELLE-PROPELLER DIAMETER RATIO ON BODY INTERFERENCE AND ON PROPELLER AND COOLING CHARACTERISTICS**

By JAMES G. MCHUGH and ELDRIDGE H. DERRING

Langley Memorial Aeronautical Laboratory

## NATIONAL ADVISORY COMMITTEE FOR AERONAUTICS

HEADQUARTERS, NAVY BUILDING, WASHINGTON, D. C.  
LABORATORIES, Langley Field, Va.

Created by act of Congress approved March 3, 1915, for the supervision and direction of the scientific study of the problems of flight (U. S. Code, Title 50, Sec. 151). Its membership was increased to 15 by act approved March 2, 1929. The members are appointed by the President, and serve as such without compensation.

JOSEPH S. AMES, Ph. D., <i>Chairman</i> , Baltimore, Md.	ROBERT H. HINCKLEY, A. B., Chairman, Civil Aeronautics Authority.
VANNEVAR BUSH, Sc. D., <i>Vice Chairman</i> , Washington, D. C.	JEROME C. HUNSAKER, Sc. D., Cambridge, Mass.
CHARLES G. ABBOT, Sc. D., Secretary, Smithsonian Institution.	SYDNEY M. KRAUS, Captain, United States Navy, Bureau of Aeronautics, Navy Department.
HENRY H. ARNOLD, Major General, United States Army, Chief of Air Corps, War Department.	CHARLES A. LINDBERGH, LL. D., New York City.
GEORGE H. BRETT, Brigadier General, United States Army, Chief Matériel Division, Air Corps, Wright Field, Dayton, Ohio.	FRANCIS W. REICHLERFER, A. B., Chief, United States Weather Bureau.
LYMAN J. BRIGGS, Ph. D., Director, National Bureau of Standards.	JOHN H. TOWERS, Rear Admiral, United States Navy, Chief, Bureau of Aeronautics, Navy Department.
CLINTON M. HESTER, A. B., LL. B., Administrator, Civil Aeronautics Authority.	EDWARD WARNER, Sc. D., Greenwich, Conn.
	ORVILLE WRIGHT, Sc. D., Dayton, Ohio.

GEORGE W. LEWIS, *Director of Aeronautical Research*

JOHN F. VICTORY, *Secretary*

HENRY J. E. REID, *Engineer-in-Charge, Langley Memorial Aeronautical Laboratory, Langley Field, Va.*

JOHN J. IDE, *Technical Assistant in Europe, Paris, France*

### TECHNICAL COMMITTEES

#### AERODYNAMICS

#### POWER PLANTS FOR AIRCRAFT

#### AIRCRAFT MATERIALS

#### AIRCRAFT STRUCTURES

#### AIRCRAFT ACCIDENTS

#### INVENTIONS AND DESIGNS

*Coordination of Research Needs of Military and Civil Aviation*

*Preparation of Research Programs*

*Allocation of Problems*

*Prevention of Duplication*

*Consideration of Inventions*

LANGLEY MEMORIAL AERONAUTICAL LABORATORY  
LANGLEY FIELD, VA.

Unified conduct, for all agencies, of scientific research on the fundamental problems of flight.

OFFICE OF AERONAUTICAL INTELLIGENCE  
WASHINGTON, D. C.

Collection, classification, compilation, and dissemination of scientific and technical information on aeronautics.

## REPORT No. 680

### THE EFFECT OF NACELLE-PROPELLER DIAMETER RATIO ON BODY INTERFERENCE AND ON PROPELLER AND COOLING CHARACTERISTICS

By JAMES G. MCHUGH and ELDRIDGE H. DERRING

#### SUMMARY

An investigation was conducted in the N. A. C. A. 20-foot tunnel to determine the slipstream drag, the body interference, and the cooling characteristics of nacelle-propeller combinations with different ratios of nacelle diameter to propeller diameter. Four combinations of geometrically similar propellers and nacelles, mounted on standard wing supports, were tested with values of the ratio of nacelle diameter to propeller diameter of 0.25, 0.33, and 0.44.

The results show that (1) the effect of variation in the ratio of nacelle diameter to propeller diameter on propulsive efficiency is not important until the nacelle becomes approximately one-third of the propeller diameter but, beyond that point, the propulsive efficiency decreases rapidly with further increase in relative body size; (2) the net efficiency of a nacelle-propeller combination decreases rapidly with increasing values of the ratio of nacelle diameter to propeller diameter; (3) the presence of a spinner over the propeller hub increases the propulsive efficiency by an amount varying from 1½ to 4 percent; and (4) the maximum pressure drop available with adjustable cowling flaps is about 20 percent greater than the maximum pressure drop available with an adjustable-length cowling skirt.

#### INTRODUCTION

Considerable information has recently been made available concerning the propulsive and the cooling characteristics of a full-scale air-cooled radial-engine nacelle-propeller combination having a ratio of the nacelle diameter to the propeller diameter of approximately 0.43. Very little information is available concerning the effects of variation of that ratio on the slipstream drag, the body interference, and the efficiencies of a propeller-nacelle combination or on the cooling-air-flow characteristics of a nacelle-propeller combination.

Most present-day estimates of the variation in propulsive efficiency with the ratio of nacelle diameter to propeller diameter are based on the results reported in references 1 and 2. Those investigations were conducted with an uncoupled radial engine and low-pitch propellers, and the results are not applicable to present practice. Only a few isolated tests are available for

determining the effect of variation in the ratio of nacelle diameter to propeller diameter on the cooling-air-flow characteristics.

In order to supply additional information on this subject, the N. A. C. A. has instituted an investigation of wing-nacelle-propeller interference and cooling characteristics. The investigation includes: (a) determinations of the drag and of the propeller and cooling characteristics of four combinations of geometrically similar model propellers and nacelles having values of the ratio of nacelle diameter to propeller diameter of 0.25, 0.33, and 0.44; and (b) determinations of the lift, the drag, and the propeller and cooling characteristics of the same combinations of propellers and nacelles operating in conjunction with a 5- by 15-foot N. A. C. A. 23018 airfoil. This report presents the results of part (a); part (b) is reported in reference 3.

The present report gives the results obtained from tests of geometrically similar 3-blade propellers of diameter  $D$  of 36 and 48 inches (3 and 4 feet) operating in conjunction with geometrically similar nacelles of diameter  $d$  of 12 and 16 inches, making possible the  $d/D$  ratios of 0.25, 0.33, and 0.44. Results obtained from other tests in which free-propeller conditions were approached are also presented. The effects of a variation in the ratio of nacelle diameter to propeller diameter on the propeller characteristics and on the slipstream drag as well as the effects of nacelle interference on propeller power and thrust are shown. Also included are the results of determinations of the cooling characteristics of all the combinations tested in addition to comparisons, on one nacelle, of adjustable cowling flaps with an adjustable-length cowling skirt as a means of controlled cooling.

#### APPARATUS AND METHODS

The N. A. C. A. 20-foot wind tunnel in which these tests were conducted is described in reference 4. The tests were conducted at air speeds from 20 to 80 miles per hour.

Two geometrically similar sheet-aluminum nacelles, 12 and 16 inches in diameter (fig. 1), with nose 7 of reference 5 were used in the investigation.

The engine was simulated by fine-mesh wire screens, the resistance of which had been adjusted to give the desired conductivity. The conductivity was determined from measurements of the quantity of air flow through the cowling and of the pressure drop across the

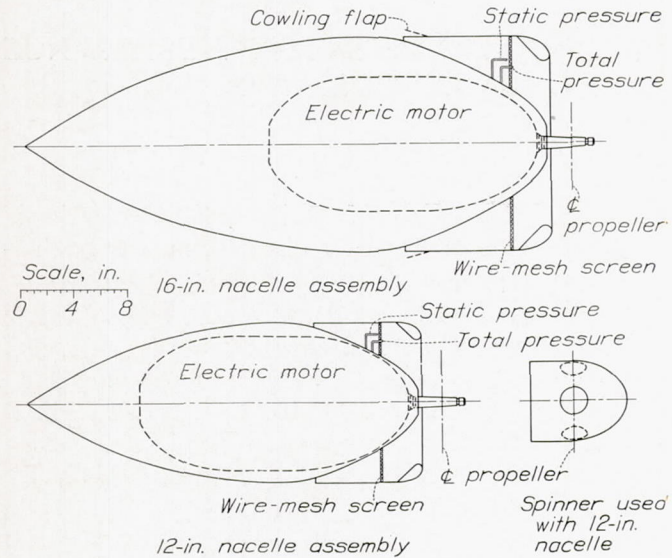


FIGURE 1.—Spinner and nacelle models used in propeller-nacelle investigation.

screens that simulated the engine. From these measurements, the conductivity  $K$  (reference 5) was found to be 0.085 for the 16-inch nacelle and 0.072 for the 12-inch nacelle.

For certain of the tests, the cowling-exit area of the 16-inch nacelle was varied both by adjusting the cowling flaps (fig. 1) and by reducing the length of the cowling skirt.

Two 3-blade propellers, 36 and 48 inches in diameter, having Clark Y sections and geometrically similar to propeller 6101 (reference 5) except for variable- instead of controllable-pitch hubs, were used in the investigation. The pitch of both propellers could be adjusted by turning the blades in the hub. For these tests, the blades were set at  $15^\circ$ ,  $20^\circ$ ,  $25^\circ$ ,  $30^\circ$ ,  $35^\circ$ , and  $40^\circ$  at 0.75 of the tip radius. Characteristic curves of blade width, blade thickness, and pitch distribution are given in figure 2.

The spinner shown in figure 1 was tested in conjunction with the 48-inch propeller and the 12-inch nacelle.

The propellers were driven by a water-cooled alternating-current induction motor, which developed 25 horsepower at 3,600 r. p. m. Current was supplied to the motor by a variable-frequency alternator and speed control was obtained by varying the frequency. The power output of the motor was obtained from a calibration involving motor torque, revolution speed, and active current.

The test set-ups were mounted in the air stream on the standard airfoil supports (reference 6) and all thrust and

drag forces were measured by automatic recording balances on the test-chamber floor.

For that portion of the test program in which it was desired to obtain free-propeller characteristics, the propeller was driven through a 3-foot extension shaft. The motor with its extension shaft was supported between the standard airfoil supports as shown in figure 3. The complete assembly was shielded from the air stream by a metal fairing that was supported from the fixed shields around the airfoil supports (fig. 4). The characteristics of the propeller alone when operating in the presence of the nacelles were obtained by attaching the nacelles to the extension-shaft fairing behind the propeller.

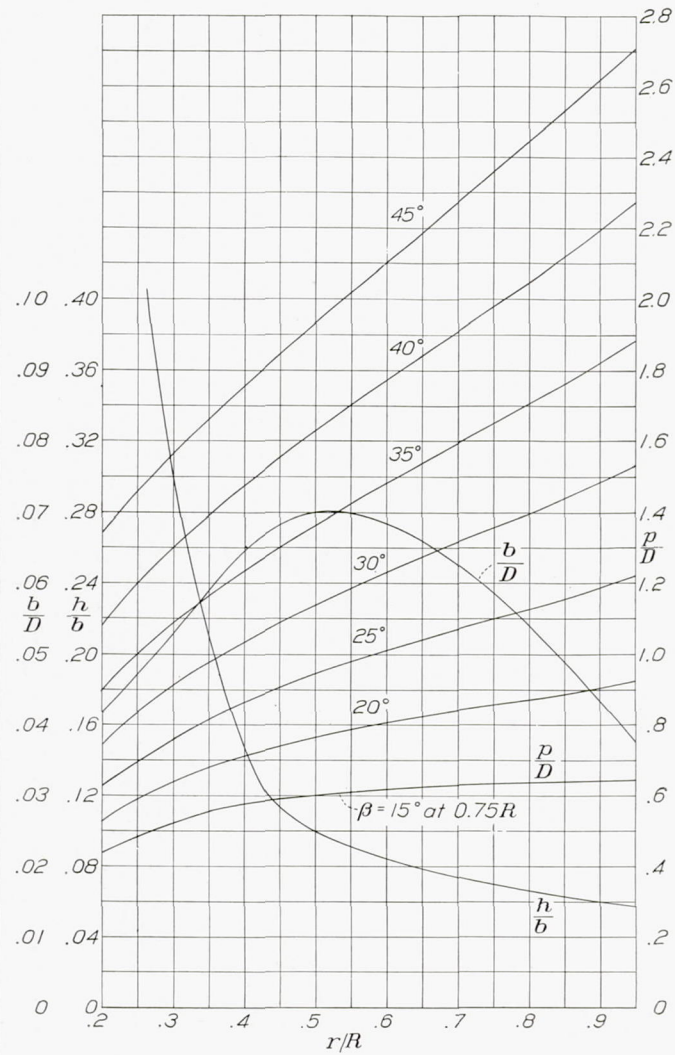
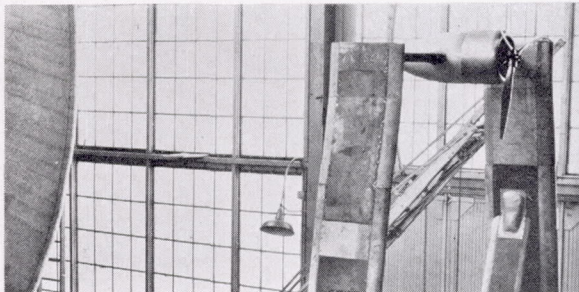
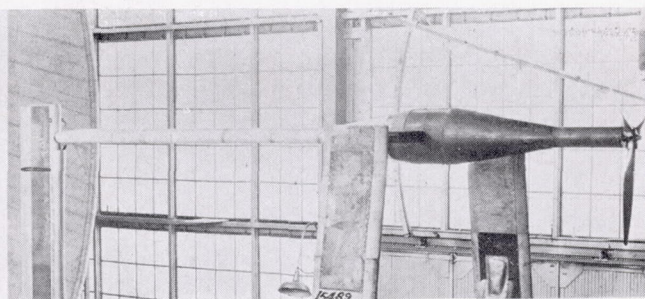


FIGURE 2.—Blade-form curves for propellers tested.  $D$ , diameter;  $R$ , radius to the tip;  $r$ , station radius;  $b$ , section chord;  $h$ , section thickness;  $p$ , geometric pitch;  $\beta$ , blade angle.

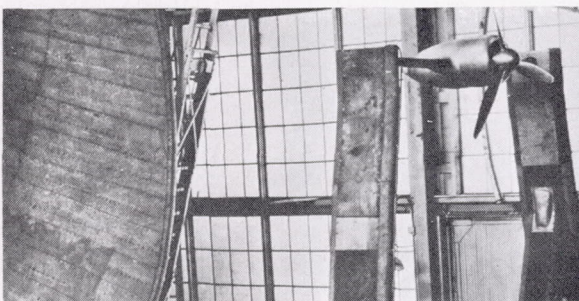
The extension shaft was not used for the tests of the nacelle-propeller units. The motor was built into the nacelle and was supported between the airfoil supports as shown in figure 3. At the beginning of this part of the test program, the supporting strut (which will subsequently be called strut 1) was large and made a bad intersection with the nacelle, thereby causing separation



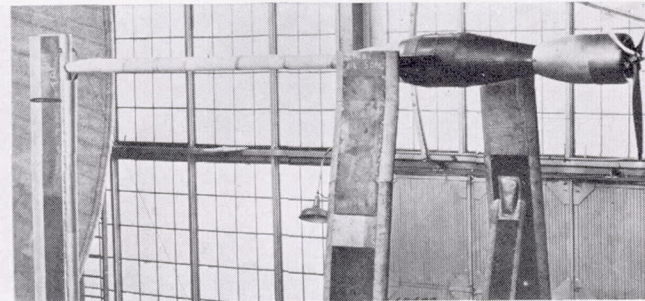
The 12-inch nacelle.



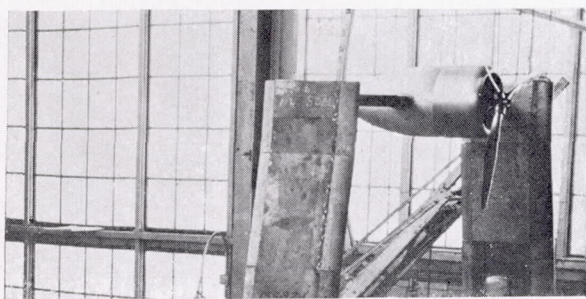
The propeller alone.



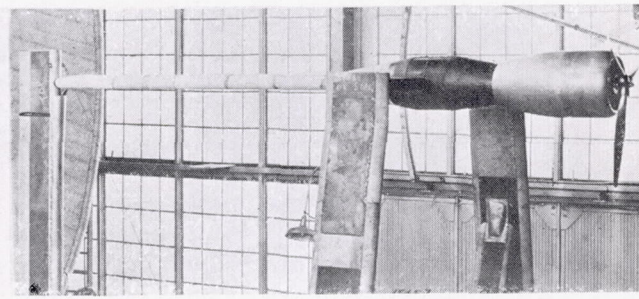
The 12-inch nacelle with spinner.



The propeller in the presence of the 12-inch nacelle.



The 16-inch nacelle.



The propeller in the presence of the 16-inch nacelle.

FIGURE 3.—Nacelle arrangements tested.

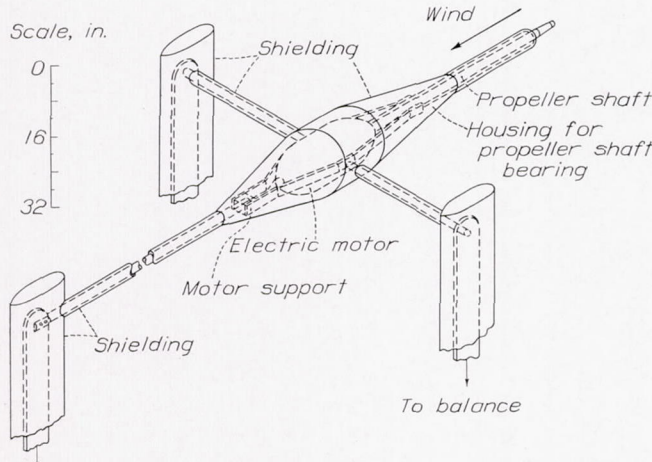


FIGURE 4.—Set-up for tests of free propeller.

of the air flow over all that portion of the nacelle behind the strut and producing unreasonably high values of the nacelle drag. Strut 1 was later replaced with a much

smaller strut (subsequently called strut 3), which was well filleted at its juncture with the nacelle and which gave no indication of causing separation of the air flow over the nacelle.

With each nacelle and cowling arrangement, a test was made with the propeller removed. Readings of the drag and of the pressure drop through the cowling were taken at various air speeds from 20 to 80 miles per hour. The propeller was then installed on the motor shaft, and tests were made with the propeller operating. During these tests, the propeller revolution speed was held constant and the air speed was varied until the maximum air speed available was reached; the air speed was then held constant and the propeller revolution speed was varied to cover the rest of the propeller operating range. Simultaneous readings of power, thrust, revolution speed, air speed, and pressure drop through the engine were taken at frequent intervals.

The tare drag of the supports was determined by attaching to the nacelle a single dummy strut, geometrically similar to the ones that supported the nacelle. Drag tests were made with and without the dummy strut in place. The tare drag was then determined on the assumption that the increase in drag due to the presence of the dummy strut was one-half of the total strut and interference drag. The tare drag with the propeller operating was not determined.

The nacelle arrangements tested are shown in figure 3.

The various combinations on which measurements of propeller characteristics were obtained are listed in the following table.

	Propeller diameter (in.)	Nacelle diameter (in.)	Cowling-flap angle (deg.)	Blade angle at 0.75R (deg.)					
Motor and supports shielded.	36	No nacelle	0	15	20	25	30	35	40
	36	12	0	15	20	25	30	35	40
	36	16	0	15	20	25	30	35	40
	48	No nacelle	0	15	20	25	30	35	40
	48	12	0	15	20	25	30	35	40
	48	16	0	15	20	25	30	35	40
	36	16	0	15	20	25	30	35	40
	48	16	0	15	20	25	30	35	40
	48	16	5	15	20	25	30	35	40
	48	16	10	15	20	25	30	35	40
Motor and nacelle supported by strut 1.	48	16	15	15	20	25	30	35	40
	48	16	20	15	20	25	30	35	40
	36	12	0	15	20	25	30	35	40
	48	12	0	15	20	25	30	35	40
	36	16	0	15	20	25	30	35	40
	48	12	0	15	20	25	30	35	40
	48	16	0	15	20	25	30	35	40
	48	16	5	15	20	25	30	35	40
	48	16	10	15	20	25	30	35	40
	48	16	15	15	20	25	30	35	40
Motor and nacelle supported by strut 3.	48	12	0	15	20	25	30	35	40
	a 48	12	0	15	20	25	30	35	40
	36	16	0	15	20	25	30	35	40
	48	16	0	15	20	25	30	35	40
	48	16	5	15	20	25	30	35	40

<sup>a</sup> With spinner.

In order to determine the relative drag and the cooling-air-flow characteristics of the nacelle when the cowling-exit area was varied, additional tests with propeller removed were made of the 16-inch nacelle. The tests were made with the cowling flaps (fig. 1) set at different angles and with a series of cowlings with different skirt lengths.

#### SYMBOLS AND COEFFICIENTS

The symbols and coefficients used in the report are defined as follows:

$q$ , dynamic pressure of air ( $\frac{1}{2}\rho V^2$ ).

$\rho$ , mass density of air.

$V$ , velocity of air stream.

$n$ , propeller revolution speed.

$Q$ , aerodynamic torque of propeller.

$D_n$ , drag of cowling-nacelle unit with propeller removed.

$\Delta D$ , change in body drag due to propeller slipstream.

$R$ , net force on thrust balance.

$T$ , thrust of propeller operating in presence of body (tension in crankshaft).

$T_f$ , propeller thrust in free air (no body).

$\Delta T$ , change in propeller thrust due to influence of body ( $T - T_f$ ).

$d$ , diameter of body behind propeller.

$D$ , diameter of propeller.

$d/D$ , ratio of nacelle diameter to propeller diameter.

$P$ , power supplied to propeller ( $2\pi Qn$ ).

$\beta$ , propeller blade angle at 0.75 radius.

$C_{D_n}$ , nacelle drag coefficient  $\left[ \frac{D_n}{q(\pi d^2/4)} \right]$ .

$T_c$ , propulsive thrust-loading coefficient  $\left( \frac{T - \Delta D}{\rho V^2 D^2} \right)$ .

$T_{ca}$ , apparent propeller thrust-loading coefficient  $(T/\rho V^2 D^2)$ .

$T_{cf}$ , free-propeller thrust-loading coefficient  $(T_f/\rho V^2 D^2)$ .

$T_{c\Delta D}$ , slipstream-drag coefficient  $(\Delta D/\rho V^2 D^2)$ .

$\Delta T_c$ , body-interference thrust coefficient  $(\Delta T/\rho V^2 D^2)$ .

$C_T$ , propulsive thrust coefficient  $\left( \frac{T - \Delta D}{\rho n^2 D^4} \right)$ .

$C_{Ta}$ , apparent propeller thrust coefficient  $(T/\rho n^2 D^4)$ .

$C_{Tf}$ , free-propeller thrust coefficient  $(T_f/\rho n^2 D^4)$ .

$C_{T_0}$ , net thrust coefficient  $\left( \frac{T - \Delta D - D_n}{\rho n^2 D^4} \right)$ .

$C_P$ , power coefficient  $(P/\rho n^3 D^5)$ .

$\eta_a$ , apparent propeller efficiency  $(TV/P)$ .

$\eta_f$ , free-propeller efficiency  $(T_f V/P)$ .

$\eta$ , propulsive efficiency  $\left[ \frac{(T - \Delta D)V}{P} \right]$ .

$\eta_0$ , net efficiency  $\left[ \frac{(T - \Delta D - D_n)V}{P} \right]$ .

$\eta_{max}$ , envelope propulsive efficiency from  $C_s$  design chart.

$V/nD$ , advance-diameter ratio of propeller.

$C_s$ , speed-power coefficient  $(\sqrt[5]{\rho V^5 / P n^2})$ .

$P_c$ , power disk-loading coefficient  $(4P/\pi D^2 q V)$ .

$K$ , conductivity of the engine (reference 5).

$\Delta p$ , pressure drop across engine.

$\sqrt{\Delta p / \rho n^2 D^2}$ , cooling-air-flow coefficient.

$F_1, F_2, F_3$ , body-interference factors.

#### RESULTS AND DISCUSSION

A study was made of the effects of variation in the value of the ratio  $d/D$  on the characteristics of a series of nacelle-propeller combinations, and the results are presented. First presented are the propeller characteristics obtained at various values of the ratio  $d/D$  and an analysis of the values to determine the magnitude of the mutual interferences that exist between the propeller and the nacelle. The cooling characteristics at the same values of  $d/D$  and, in addition, the results of incidental tests to determine the effect of various types of control of cowling-exit area on cooling-air flow are then presented.

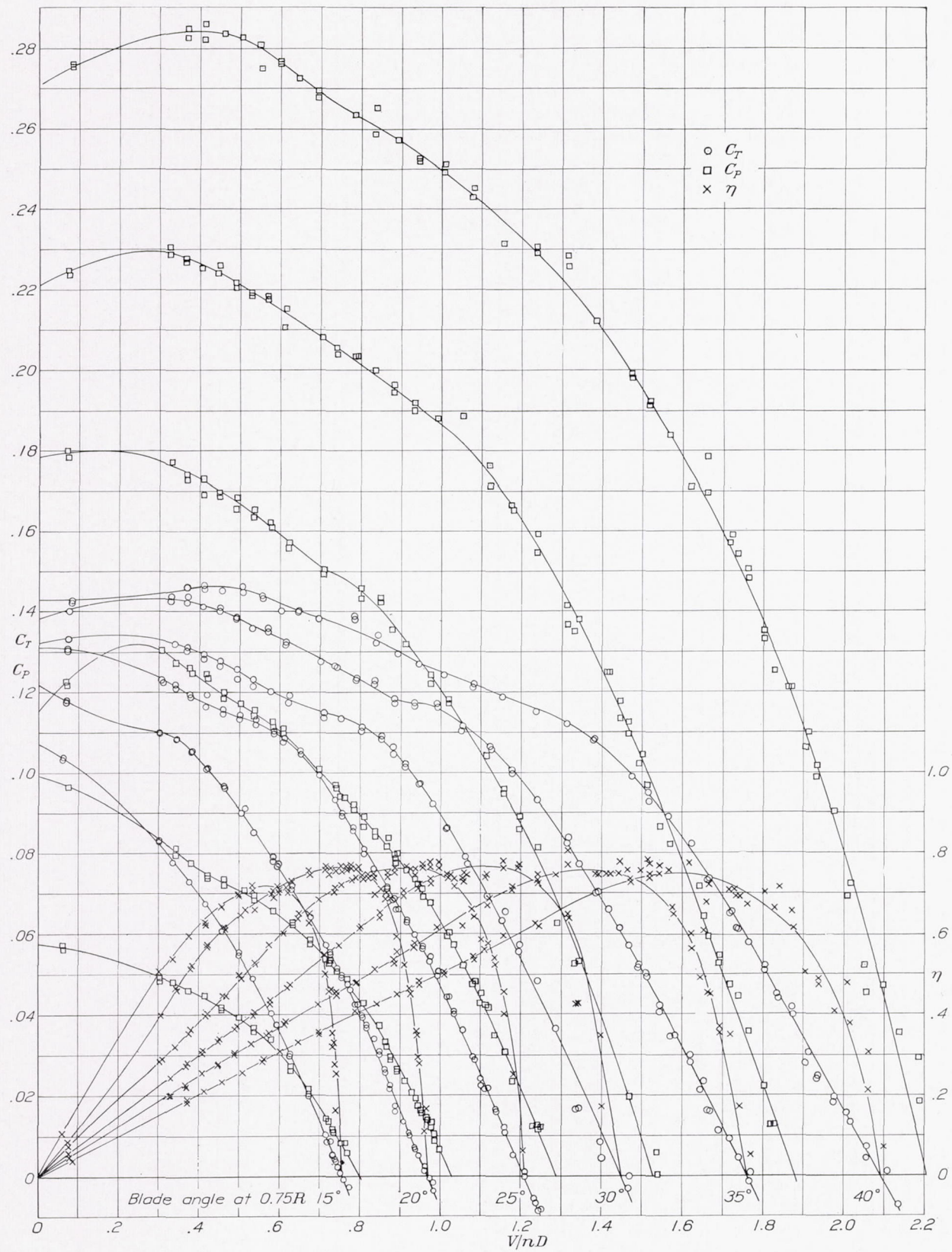


FIGURE 5.—Typical propeller-test results for six blade angles; 36-inch propeller operating in conjunction with 16-inch nacelle.

## PROPELLER CHARACTERISTICS AND INTERFERENCE EFFECTS

All propeller data were reduced to the standard non-dimensional coefficients and were plotted as functions of  $V/nD$ . Representative test results are plotted in figure 5 to show the variation of the test points.

In figure 6 a comparison is made of the results of tests with two different supports for the motor nacelle. It is to be noted that a much higher value of propulsive efficiency was obtained when strut 1 was used to support the nacelle than when the nacelle was supported by

fact that misleading results may be obtained from tests of propellers in conjunction with bodies of such form as to allow the critical flow condition encountered with strut 1 to occur. The ensuing analyses of propeller characteristics in this report are based on test results obtained when the nacelle was supported by strut 3. With this supporting arrangement, any discrepancy in the results due to the effect of strut interference is believed to be quite small.

In order to show the over-all effects of variation in

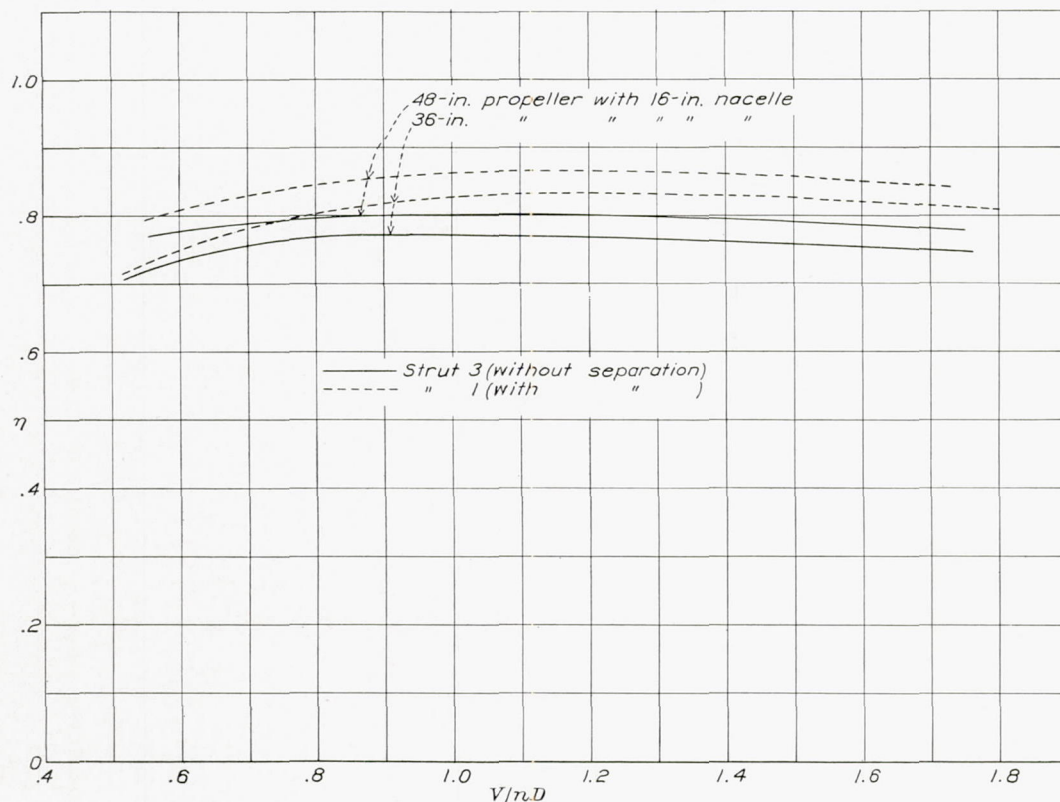


FIGURE 6.—Effect of strut interference on envelope curves of propulsive efficiency.

strut 3. The cause of this difference in propulsive efficiency was determined from a study of the air flow over the nacelle by attaching streamers to its surface and studying their actions in the air stream with and without the propeller operating. When the nacelle was supported by strut 1 with the propeller removed, the air flow separated over all that portion of the nacelle back of the strut intersection but, with the propeller operating, the effect of the slipstream was to shift the separation point downstream by several inches. The slipstream thus caused an effective reduction in nacelle drag and a high value of propulsive efficiency was therefore obtained. A similar study of the flow when the nacelle was supported by strut 3 revealed that the separation point was near the tail and was apparently uninfluenced by the propeller slipstream.

As a result of this study, it is desired to stress the

$d/D$  on the efficiencies of the nacelle-propeller combinations, the envelope curves of apparent, propulsive, and net efficiency for the various arrangements tested are given as a function of  $V/nD$  in figure 7 and as a function of  $C_s$  in figure 8. Attention is called to the fact that the results given for values of  $d/D$  of 0.10 and 0.13 in figures 7 and 8 were obtained from tests with no nacelle behind the propeller. In those cases, the value of  $d/D$  is the ratio of the diameter of the extension-shaft fairing to the propeller diameter.

The increase in both propulsive and net efficiency that can be obtained through the use of a spinner is also shown in figures 7 and 8. At the value of  $d/D$  of 0.25, at which tests were made with a spinner over the propeller hub, the gain obtained varied from about 1 percent in the take-off range to about 4 percent in the high-speed range.

Figure 9 summarizes the results given in figures 7 and 8 and illustrates quite clearly the variation at both constant  $V/nD$  and constant  $C_s$  of the various efficiencies

rapid decrease in net efficiency with increasing values of  $d/D$ . The divergence of the two sets of curves from each other is explained on the premise that, although

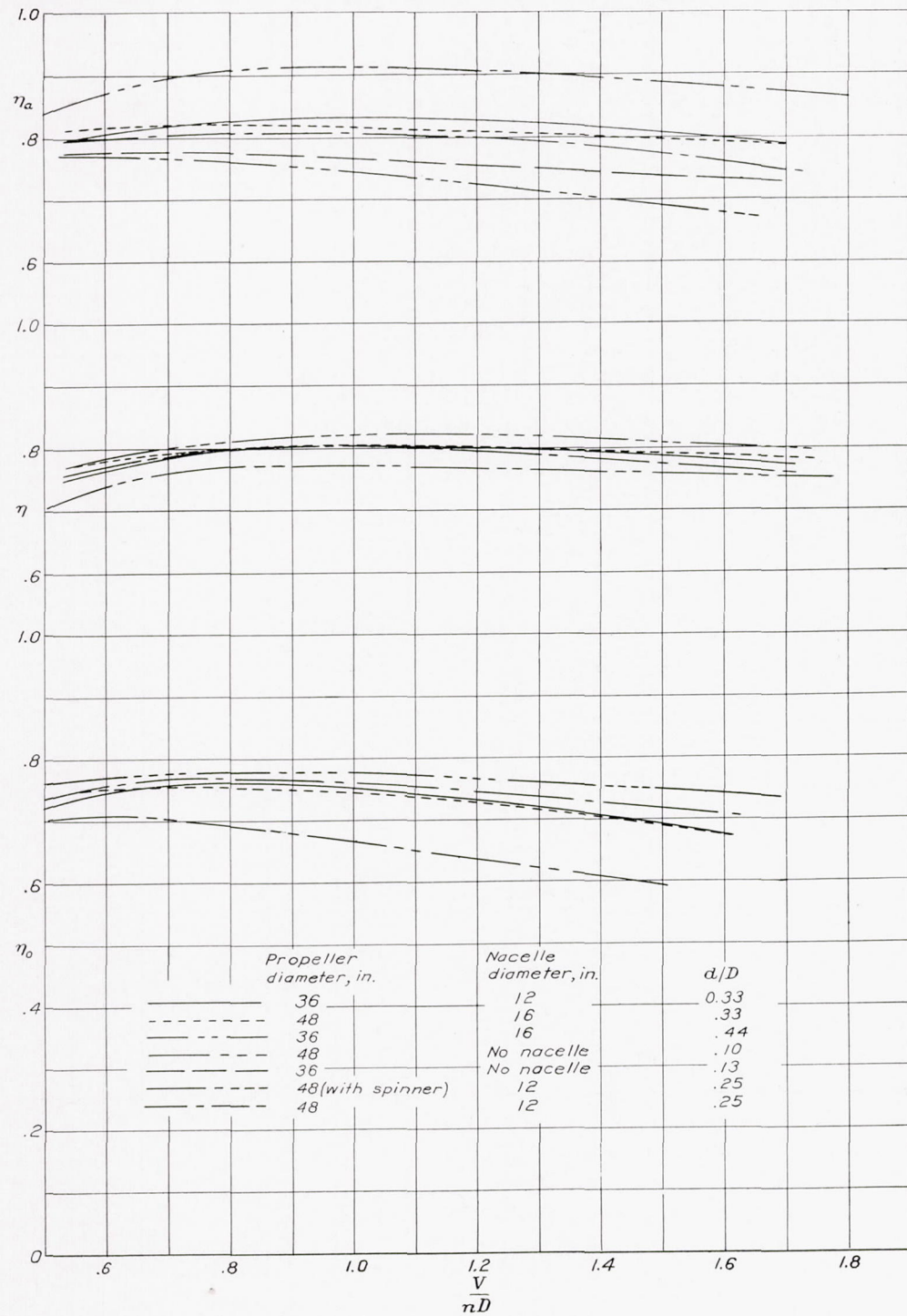


FIGURE 7.—The variation of apparent, propulsive, and net efficiency envelopes with  $V/nD$ .

with relative body size. The chosen values of  $V/nD$  and  $C_s$  roughly correspond to the take-off and cruising conditions of a representative transport airplane. There is a rapid increase in apparent efficiency and a

the increase in body size causes an increase in apparent thrust owing to the greater reaction created between body and propeller, the net thrust of the combination has been reduced owing to the increase in body drag.

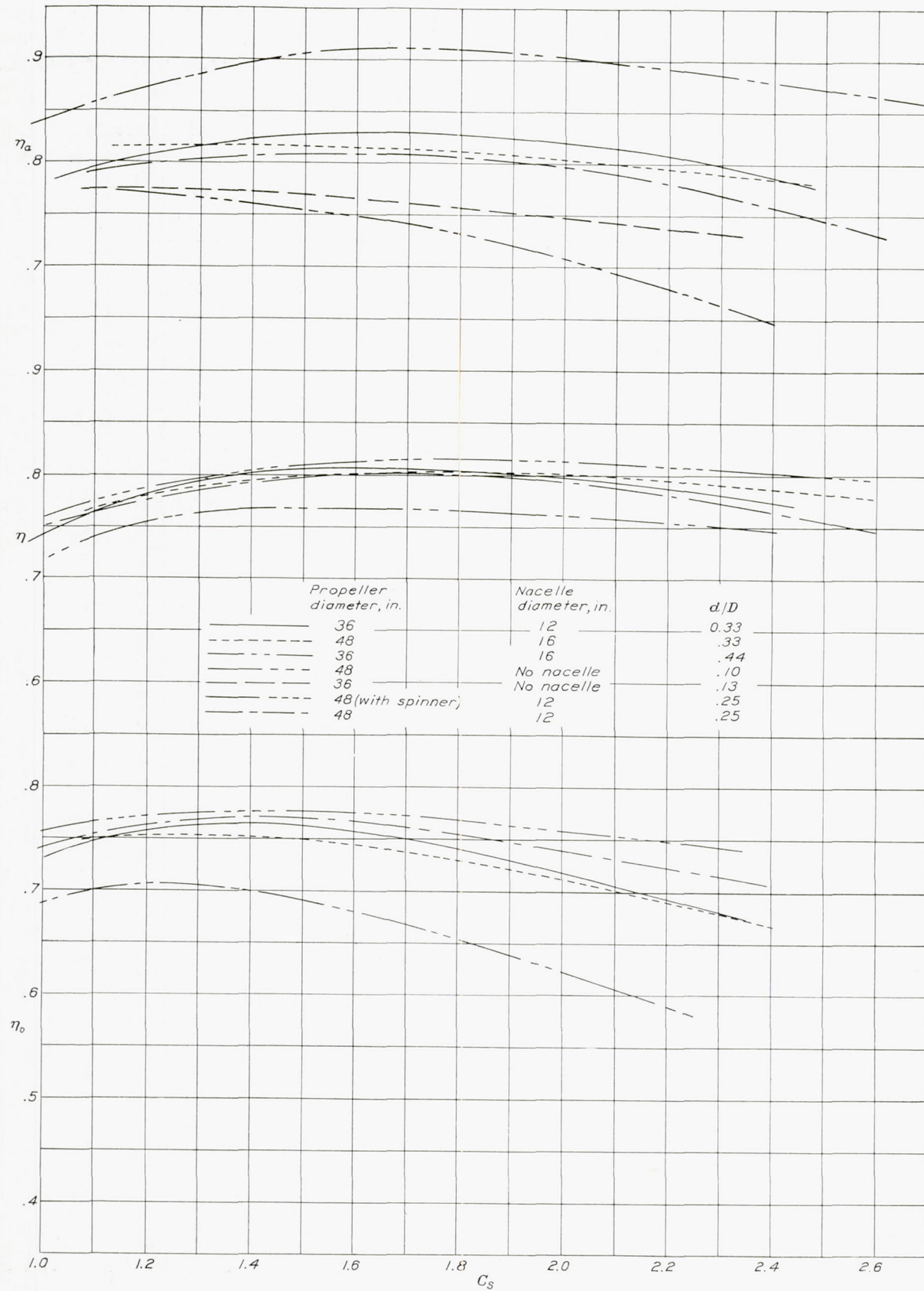
FIGURE 8.—The variation of apparent, propulsive, and net efficiency envelopes with  $C_s$ .

Figure 10 is presented to show the effect of the  $d/D$  ratio on the parameters that influence the selection of a propeller. The ideal efficiency of a propeller is directly dependent on power disk loading. The effect of change in value of  $d/D$  is, in turn, to alter the power disk loading. The use of the power disk-loading coefficient  $P_c$  as the independent variable in figure 10 is therefore very convenient in that it allows comparisons of the other important design coefficients at a constant value of power disk loading. The other coefficients shown in figure 10 were obtained from design charts of the type shown in figure 11 and from similar charts in which  $1/\sqrt[3]{P_c}$  was the independent variable. Figure 10 is of extreme interest because it shows in concise form, for all the combinations tested with strut 3, the following important information:  $C_s$  at  $V/nD$  for  $\eta_{max}$ ;  $V/nD$  for  $\eta_{max}$ ; and the values of  $\eta_{max}$  and  $\beta$  that are usually obtained from the conventional  $C_s$  design charts. At the same time it permits their comparison at a constant value of power disk loading.

The values of  $\eta_{max}$  obtained at  $d/D=0.33$  are nearly the same as those obtained at  $d/D=0.25$ . The difference is of the order of one-half of 1 percent and may be within the experimental error of the results. At the lower ratio, however, there may be a loss in propulsive efficiency owing to the fact that a relatively small body does not tend to make inoperative the inefficient hub and root sections of the propeller and therefore a larger portion of the power is wasted than if the propeller were operating in front of a larger body.

The propulsive efficiency obtained at  $d/D=0.44$  is of the order of 4 or 5 percent lower than that obtained at either of the other ratios. Inspection of the results given in figure 10 and of the envelope curves of propulsive efficiency given in figures 7 and 8 indicates that, for practical installations, the effect of  $d/D$  on propulsive efficiency is relatively unimportant at values of  $d/D$  less than 0.33. At higher values of  $d/D$ ,  $\eta$  decreases rapidly with increasing values of  $d/D$ . This result is in agreement with the result anticipated from extrapolation of previous test results.

The differences in propulsive efficiency that have been discussed thus far are attributed to the fact that the presence of a body behind an operating propeller has two opposing effects. The presence of the body alters the air-flow pattern through the propeller and changes its power and thrust disk loadings to different values from those which obtained when no body is present. As shown in figure 12, the propeller thrust (crankshaft tension) and power absorbed by a propeller of given diameter operating at a given velocity, revolution speed, and blade angle are not the same when the propeller operates in the presence of a body as they are when the propeller operates in a free air stream. This effect is herein referred to as a "body-interference" effect. The presence of the body in the slipstream

has an additional effect owing to the fact that it is subjected to an increment of drag over and above the drag that would obtain if the propeller were not operating. This drag increment is commonly referred to as the "slipstream" drag.

The magnitudes of the body interference effects were evaluated by determining, at conditions of equal average power disk loading, the difference between the

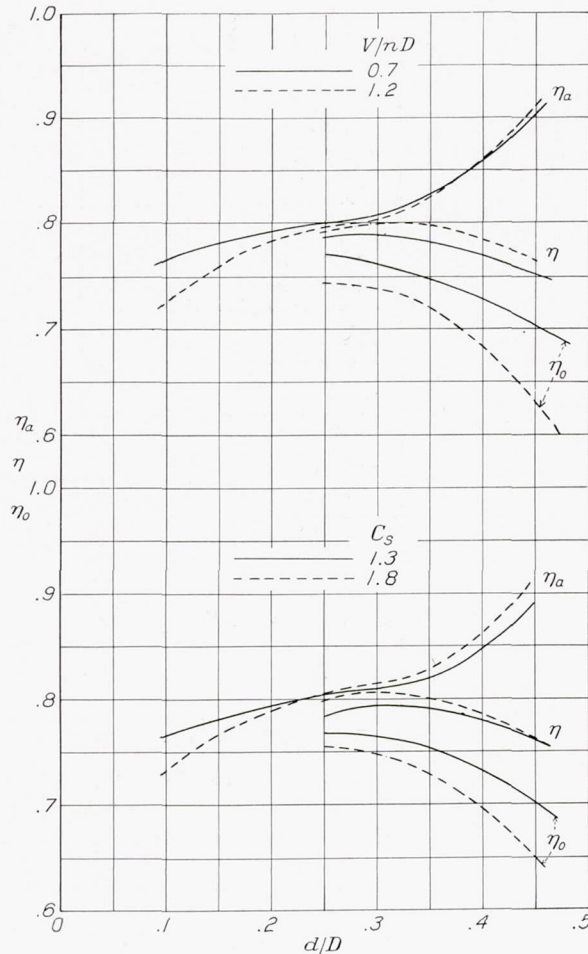


FIGURE 9.—The variation of apparent, propulsive, and net efficiency envelopes with  $d/D$ .

thrust-loading coefficient  $T_{cf}$  of the propeller in free air and the thrust-loading coefficient of the propeller subjected to body interference  $T_{ca}$ . In coefficient form, the interference thrust can be expressed as follows:

$$\Delta T_c = T_{ca} - T_{cf}$$

Figure 13 shows the variation of the body-interference thrust coefficient  $\Delta T_c$  with the free-propeller thrust-loading coefficient  $T_{cf}$  for all values of  $d/D$  and blade-angle setting at which tests were conducted. It is to be noted that, although the results for any one value of blade-angle setting follow a straight line throughout the important operating range of the propeller, the values obtained from the various blade angles depart slightly from a mean line. Insufficient data were avail-

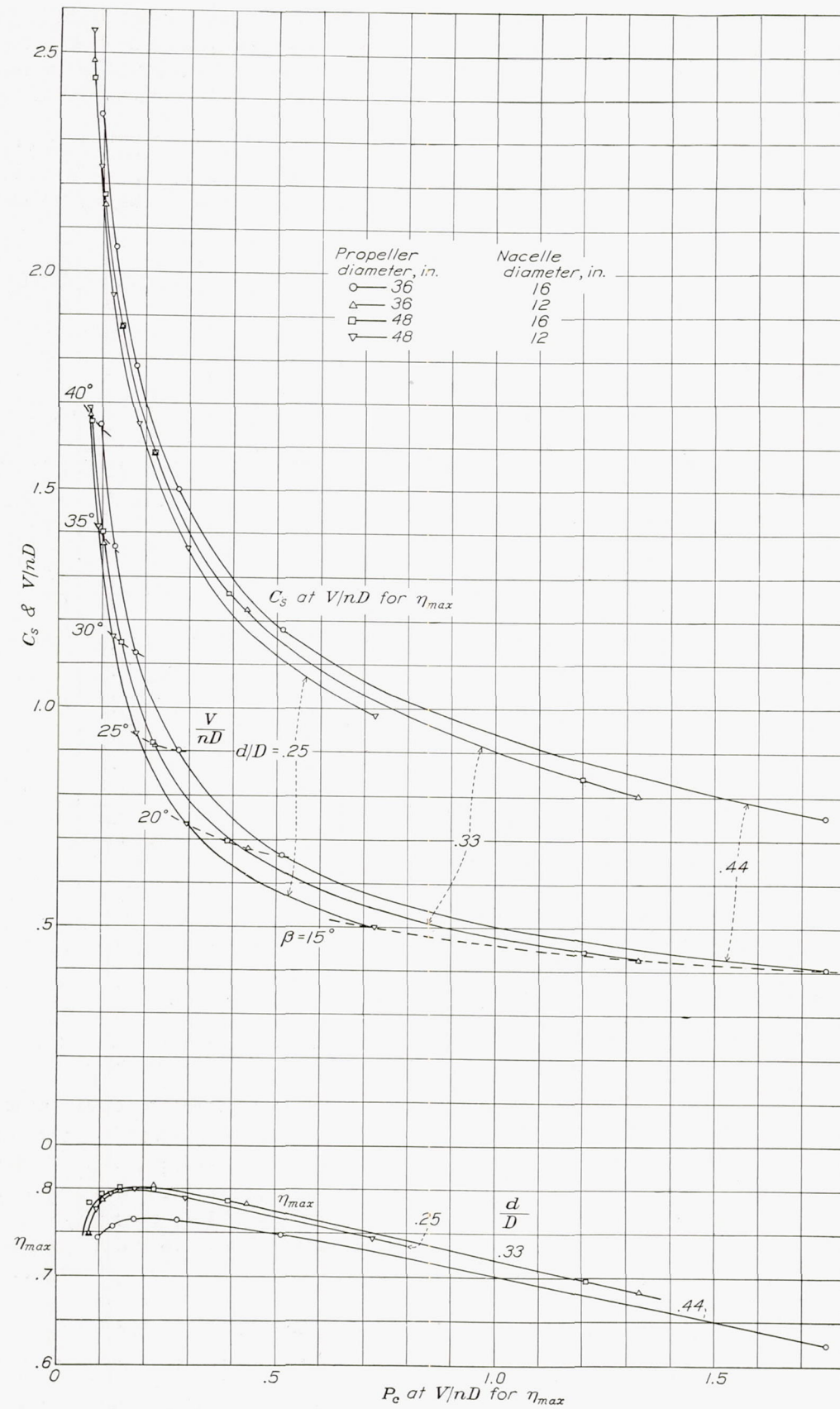


FIGURE 10.—The variation of propeller design parameters with  $P_e$  at  $V/nD$  for  $\eta_{max}$  for various values of  $d/D$ .

able to determine the secondary effects that may have caused this departure; the representation of the variation of  $\Delta T_c$  with  $T_{c_f}$  by a single straight line for all blade angles was therefore considered to be justified.

The method used to evaluate the slipstream drag was basically similar to that used to determine the body-interference effects. The slipstream drag is the differ-

tion, there can be but one value of the power coefficient at a given value of  $V/nD$ .

The variation of slipstream-drag coefficient  $T_{c_{\Delta D}}$  determined by the method previously outlined with the apparent propeller thrust-loading coefficient is shown for the various propeller-nacelle combinations in figure 14. There is considerable dispersion of the plotted points but, by the same reasoning used in the

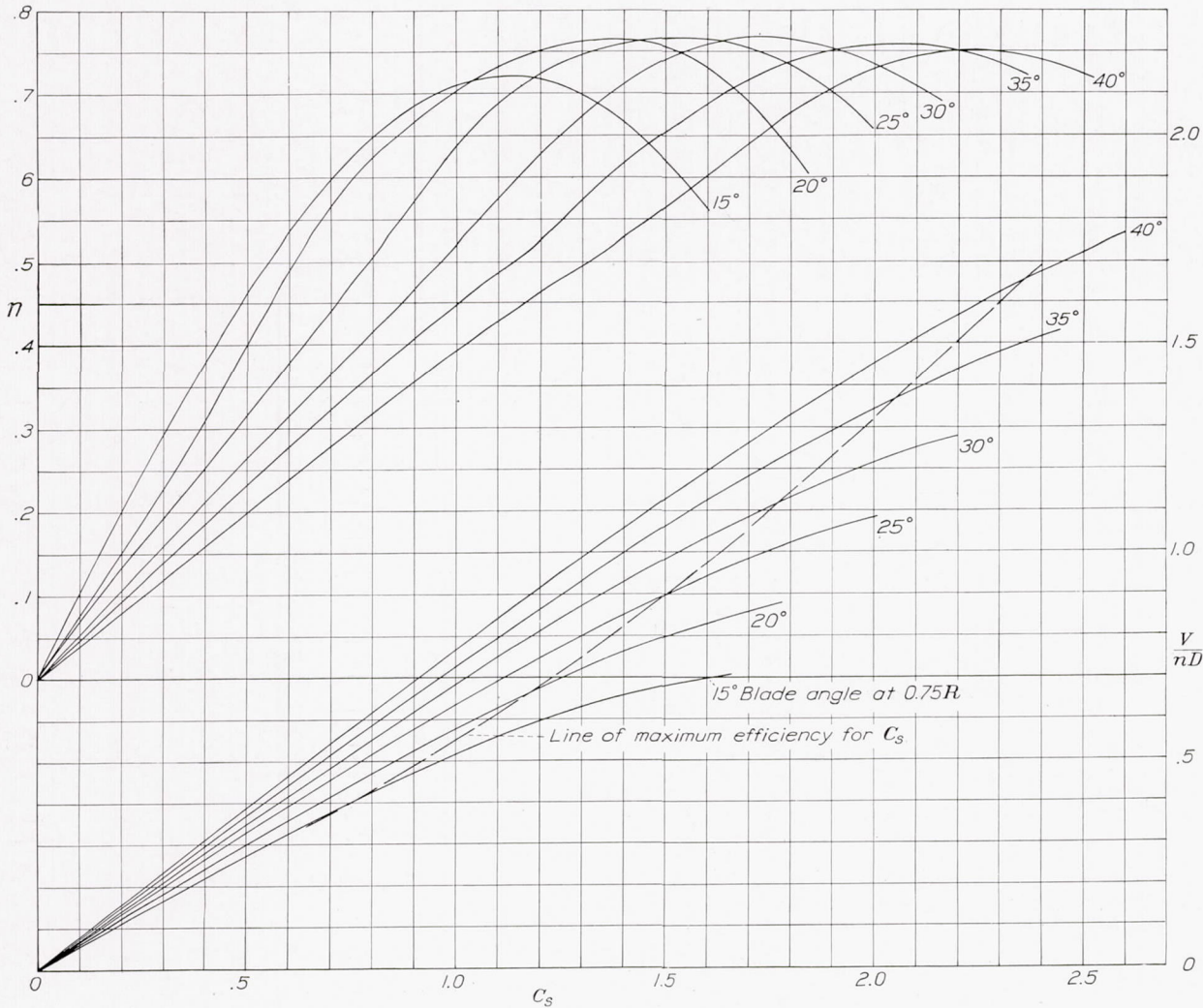


FIGURE 11.—Representative design chart; 36-inch propeller and 16-inch nacelle.

ence between the propeller thrust  $T$  and the propulsive thrust ( $T - \Delta D$ ) and, in coefficient form, can be defined as follows:

$$T_{c_{\Delta D}} = \frac{\Delta D}{\rho V^2 D^2} = \frac{T}{\rho V^2 D^2} - \frac{T - \Delta D}{\rho V^2 D^2}$$

It can be readily determined by taking the difference, at equal values of  $V/nD$ , between the apparent thrust-loading coefficient of the propeller operating in the presence of the nacelle and the propulsive thrust-loading coefficient of the propeller-nacelle combination. Such a comparison is made at equal values of the power loading because, for a given propeller-nacelle combina-

case of figure 13, the representation of the variation of  $T_{c_{\Delta D}}$  with  $T_{c_a}$  by a single straight line was considered to be justified.

Inspection of figures 13 and 14 reveals that the values of  $\Delta T_c$  and  $T_{c_{\Delta D}}$  can be expressed as follows

$$\Delta T_c = F_1 + F_2 T_{c_f} \quad (1)$$

and

$$T_{c_{\Delta D}} = F_3 T_{c_a} \quad (2)$$

In the following analysis, it will be shown that the propulsive thrust of a propeller-nacelle combination can be expressed in terms of the free-propeller thrust and the factors  $F_1$ ,  $F_2$ , and  $F_3$ .

By definition, the propulsive thrust-loading coefficient is

$$T_c = \frac{T - \Delta D}{\rho V^2 D^2}$$

Evaluating  $T_c$  in terms of  $T_{cf}$  and the interference factors gives

$$T_c = \frac{T - \Delta D}{\rho V^2 D^2} = \frac{T_f + \Delta T - \Delta D}{\rho V^2 D^2} \quad (3)$$

Substituting values from equations (1) and (2)

$$T_c = \frac{T_f}{\rho V^2 D^2} + \left( F_1 + F_2 \frac{T_f}{\rho V^2 D^2} \right) - F_3 \frac{T}{\rho V^2 D^2} \quad (4)$$

Since

$$T = T_f + \Delta T$$

then

$$\begin{aligned} T_c &= \frac{T_f}{\rho V^2 D^2} + \left( F_1 + F_2 \frac{T_f}{\rho V^2 D^2} \right) \\ &\quad - F_3 \left[ \frac{T_f}{\rho V^2 D^2} + \left( F_1 + F_2 \frac{T_f}{\rho V^2 D^2} \right) \right] \end{aligned} \quad (5)$$

Expanding and simplifying

$$T_c = \frac{T_f}{\rho V^2 D^2} (1 + F_2 - F_3 - F_2 F_3) + (F_1 - F_1 F_3) \quad (6)$$

Let

$$A = (1 + F_2 - F_3 - F_2 F_3) \quad (7)$$

$$B = (F_1 - F_1 F_3) \quad (8)$$

Then

$$T_c = AT_{cf} + B \quad (9)$$

Values of  $F_1$ ,  $F_2$ , and  $F_3$  obtained from figures 13 and 14 together with computed values of  $A$  and  $B$  are given as a function of  $d/D$  in figure 15. The values probably possess no great degree of accuracy and may be considerably different for geometrically different bodies and propellers. They are of value, however, in that they show the relative importance of the various interference factors and may therefore be useful in analyzing other test data. If other data are not available, the factors shown in figure 15 may be used to estimate the thrust characteristics at a given value of the ratio  $d/D$  when the characteristics at some other value of  $d/D$  are known.

For example, let the subscript  $x$  indicate coefficients and factors that apply to the  $d/D$  ratio for which no test data are available and let the subscript  $k$  indicate corresponding coefficients and factors that apply to the ratio for which test data are available. It can then be said that

$$T_{cx} = A_x T_{cf} + B_x \quad (10)$$

and

$$T_{ck} = A_k T_{cf} + B_k \quad (11)$$

Equating both equations to  $T_{cf}$  and solving for  $T_{cx}$ ,

$$T_{cx} = \frac{A_x}{A_k} [T_{ck} - B_k] + B_x \quad (12)$$

If  $T_{cf}$  is known,  $T_{cx}$  may be estimated by the relation given in equation (10).

It should be borne in mind that the relations developed in this analysis hold only when the various thrust coefficients involved are all taken at equal values of  $P_c$ .

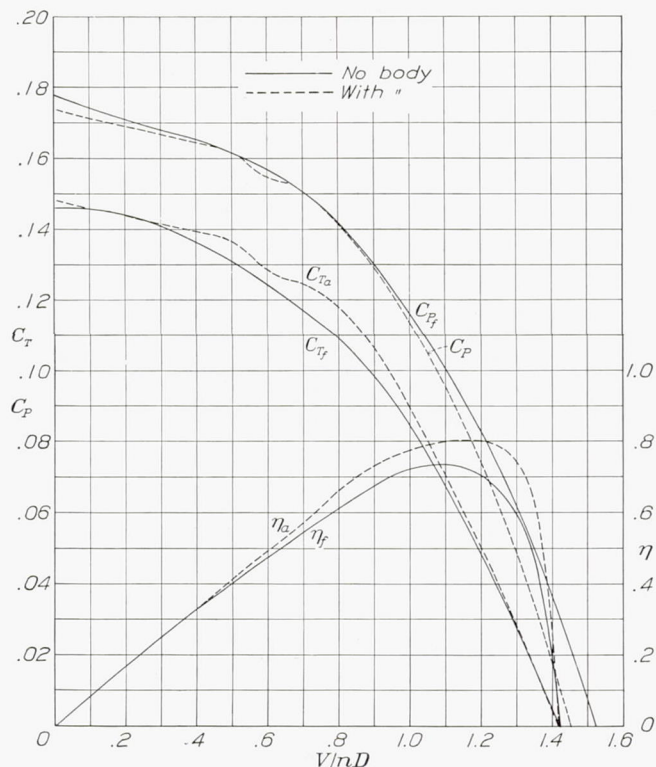


FIGURE 12.—Comparison of characteristics of 48-inch propeller in free air with characteristics of the same propeller operating in presence of 16-inch nacelle. Blade angle, 30°.

#### COOLING CHARACTERISTICS

For the presentation of the cooling characteristics, the nondimensional cooling-air flow coefficient  $\sqrt{\Delta p / \rho n^2 D^2}$  has been introduced. The values obtained from all pressure-drop measurements with the propeller operating were converted to this coefficient and plotted as a function of  $V/nD$ . Such a method of presenting the results is of advantage because it allows the results of measurements of pressure drop both with the propeller removed and with the propeller operating to be presented on the same chart. The measurements with the propeller removed can be presented as a function of  $V/nD$  in terms of  $\sqrt{\Delta p / \rho n^2 D^2}$  because on such a chart the slope of any straight line through the origin is

$$\sqrt{\frac{\Delta p}{\rho n^2 D^2}} = \frac{1}{V/nD} \sqrt{\frac{\Delta p}{q}} \quad (13)$$

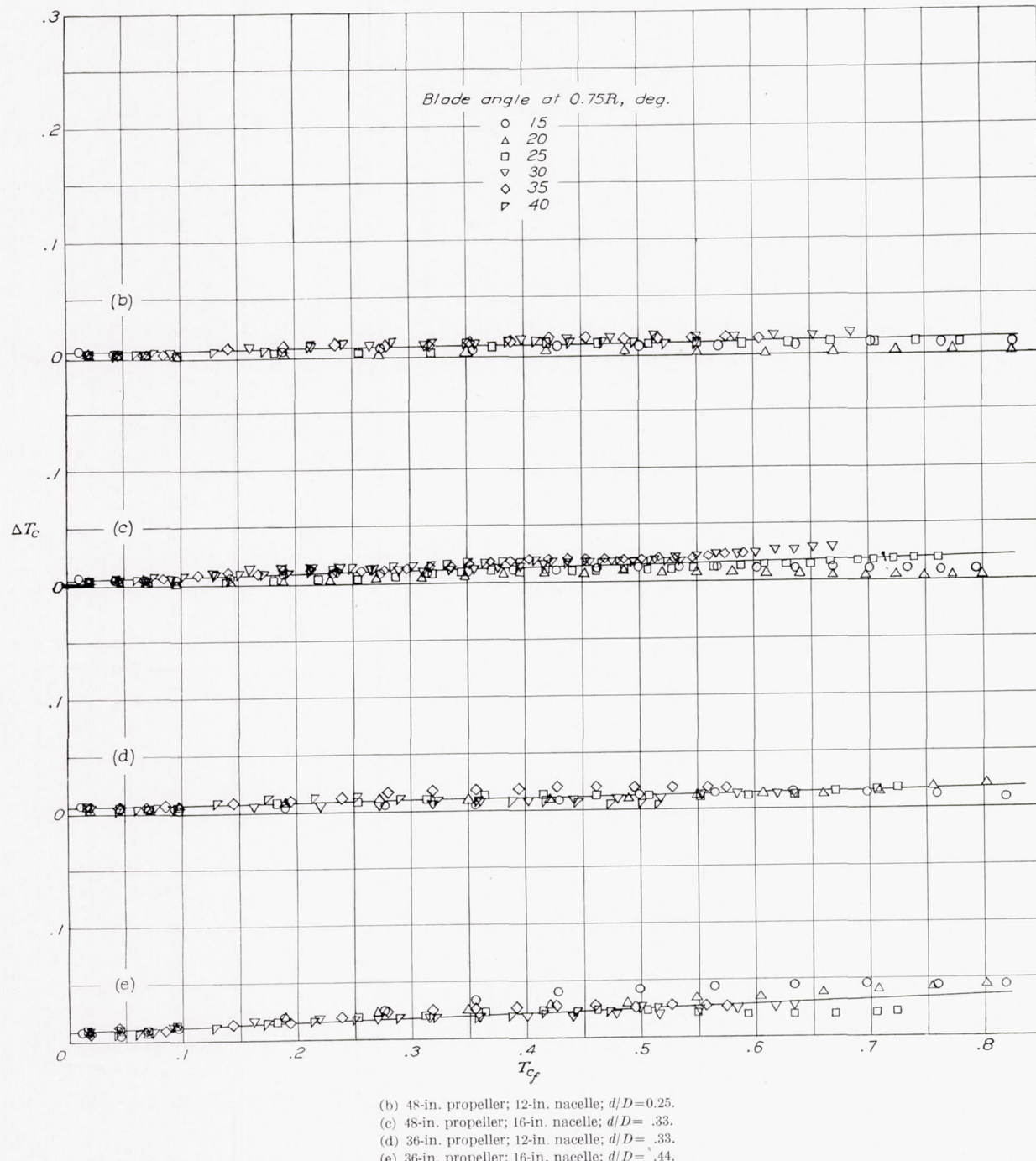


FIGURE 13.—The variation of interference-thrust coefficients with free-propeller thrust-loading coefficients.

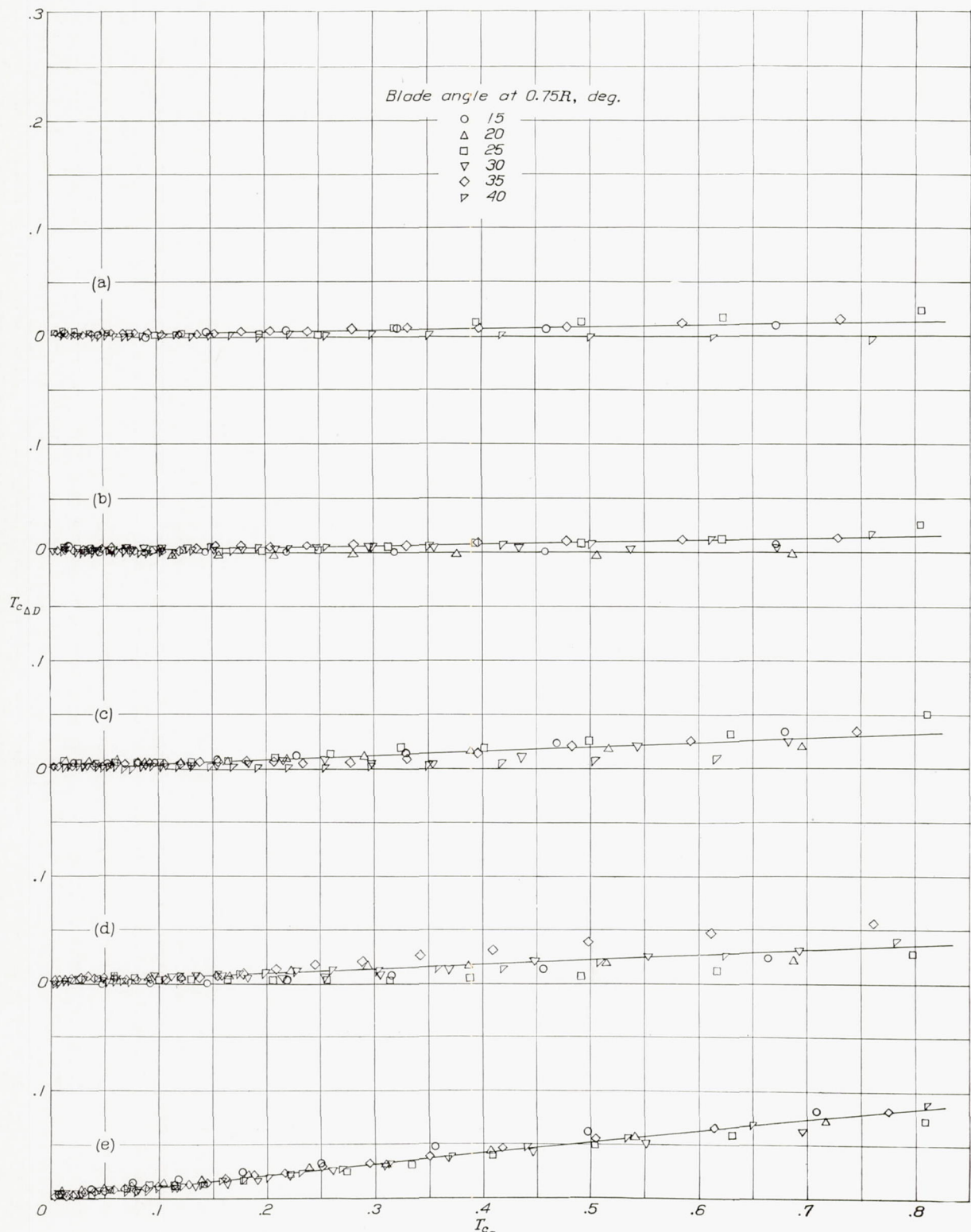
(a) 48-in. propeller; 12-in. nacelle (with spinner);  $d/D=0.25$ .(b) 48-in. propeller; 12-in. nacelle;  $d/D=.25$ .(c) 48-in. propeller; 16-in. nacelle;  $d/D=.33$ .(d) 36-in. propeller; 12-in. nacelle;  $d/D=.33$ .(e) 36-in. propeller; 16-in. nacelle;  $d/D=.44$ .

FIGURE 14.—The variation of slipstream-drag coefficients with apparent propeller thrust-loading coefficients.

Except for a slight variation with Reynolds Number, the value of  $\Delta p/q$  obtained with the propeller removed is essentially constant. By the substitution in equation (13) of the value of  $\Delta p/q$  obtained from tests with the propeller removed, an expression giving the pressure drop under that condition is obtained and a straight line satisfying this expression can be drawn on the plot of  $\sqrt{\Delta p/\rho V^2 D^2}$  against  $V/nD$ . Such a line represents, for the case under consideration, the pressure available without the effect of the propeller. From the results presented on such a chart, the pressure drop available can be determined, when  $\rho$ ,  $V$ ,  $n$ , and  $D$  are known, from equation (13) and the quantity

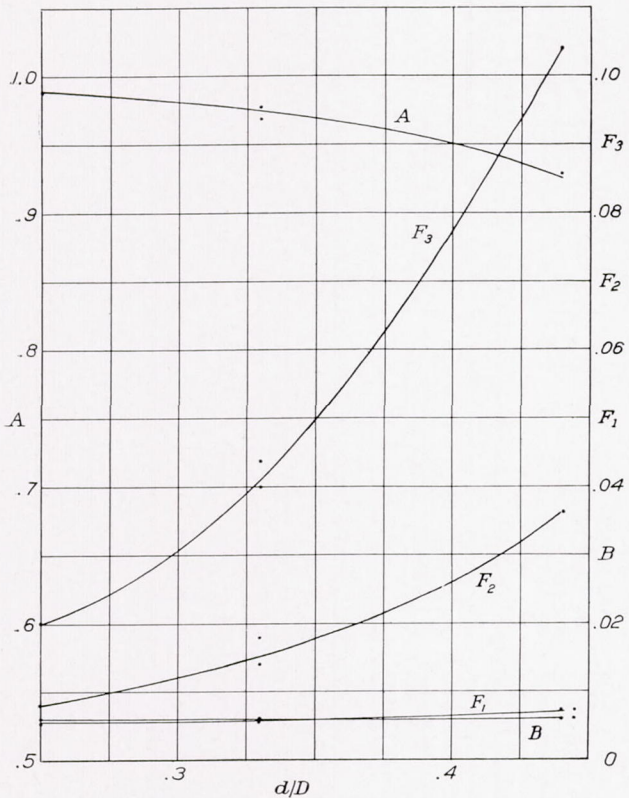


FIGURE 15.—The variation of body interference factors with  $d/D$ .

of air flow can be determined from the relation shown in equation (2) of reference 5.

The effect of variation in  $d/D$  on the cooling-air-flow coefficient is given in figure 16. The trend of the results is in agreement with that indicated by previous investigations. At high values of  $V/nD$ , i. e., high velocities, the effect of the propeller was practically the same for all blade-angle settings and, for all cases, the propeller decreased the pressure drop below the corresponding values obtained with the propeller removed. At low values of  $V/nD$ , the effect of the propeller was largely dependent on blade-angle setting and tended to increase the pressure drop, except in the extreme case shown in figure 16 (c), where the nacelle diameter was only 25 percent of the propeller diameter. In this case, the propeller showed a slightly favorable effect at high blade-angle settings but, at blade-angle settings below

25°, the propeller actually caused a reversal of flow at low values of  $V/nD$ .

It was believed that the poor cooling characteristics obtained from tests of the propeller-nacelle combination giving a value of  $d/D$  of 0.25 might be due to the fact that, at this value of the ratio, the hub was so large relative to the entrance at the front of the cowling that it was creating an adverse pressure gradient and thus causing the air to flow away from the entrance. An additional series of tests was therefore conducted on the same arrangement but with the propeller hub covered by the spinner shown in figure 1. Comparison of the results obtained with the spinner with those obtained without the spinner (fig. 16) reveals that, with the propeller operating, the spinner caused no appreciable change in the pressure-drop coefficients. This result was contrary to expectation and may be partly explained by the comparison of the pressure-drop coefficients obtained with the propeller removed and with and without the spinner in place. Further reference to figure 16 shows that the pressure drop obtained with the spinner in place was about 20 percent less than that obtained when the spinner was removed. It therefore appears that the spinner had two effects, one of which compensated for the other. It restricted the cowling entrance and caused large total-pressure entrance losses, but it improved the air flow over the hub enough to compensate for the adverse effects of restricting the entrance.

The results of tests, with the propeller operating, to determine the effect on cooling characteristics of varying the exit area by cowling flaps are presented in figure 17. For all values of  $V/nD$ , the cooling coefficient increases linearly with the cowling-exit area until the exit area becomes about 10 percent of the nacelle cross-sectional area. At larger values of the exit opening, the slope of the cooling-coefficient curves decreases rapidly until, at an exit area of about 20 percent of the cross-sectional area of the nacelle, it appears that there is but little to be gained through further increase in exit area.

The relative merits of adjustable cowling flaps and an adjustable-length cowling skirt as a means of controlling the pressure drop across the engine are compared, on the basis of test results obtained with the propeller removed, in figures 18 and 19. From figure 18, which compares the effectiveness of the two methods, it is seen that both are of about equal merit for exit areas up to about 10 percent of the engine cross-sectional area. For larger exit areas, the greater effectiveness of adjustable cowling flaps becomes increasingly important; when the exit area is 25 percent of the cross-sectional area, the cowling flaps give a value of  $\Delta p/q$  of 1.22 as compared with the value of 0.83 obtained with the adjustable-length skirt. It is of further interest to note from figure 18 that the maximum pressure attainable with cowling flaps is apparently much higher than can be obtained with an adjustable-length skirt.

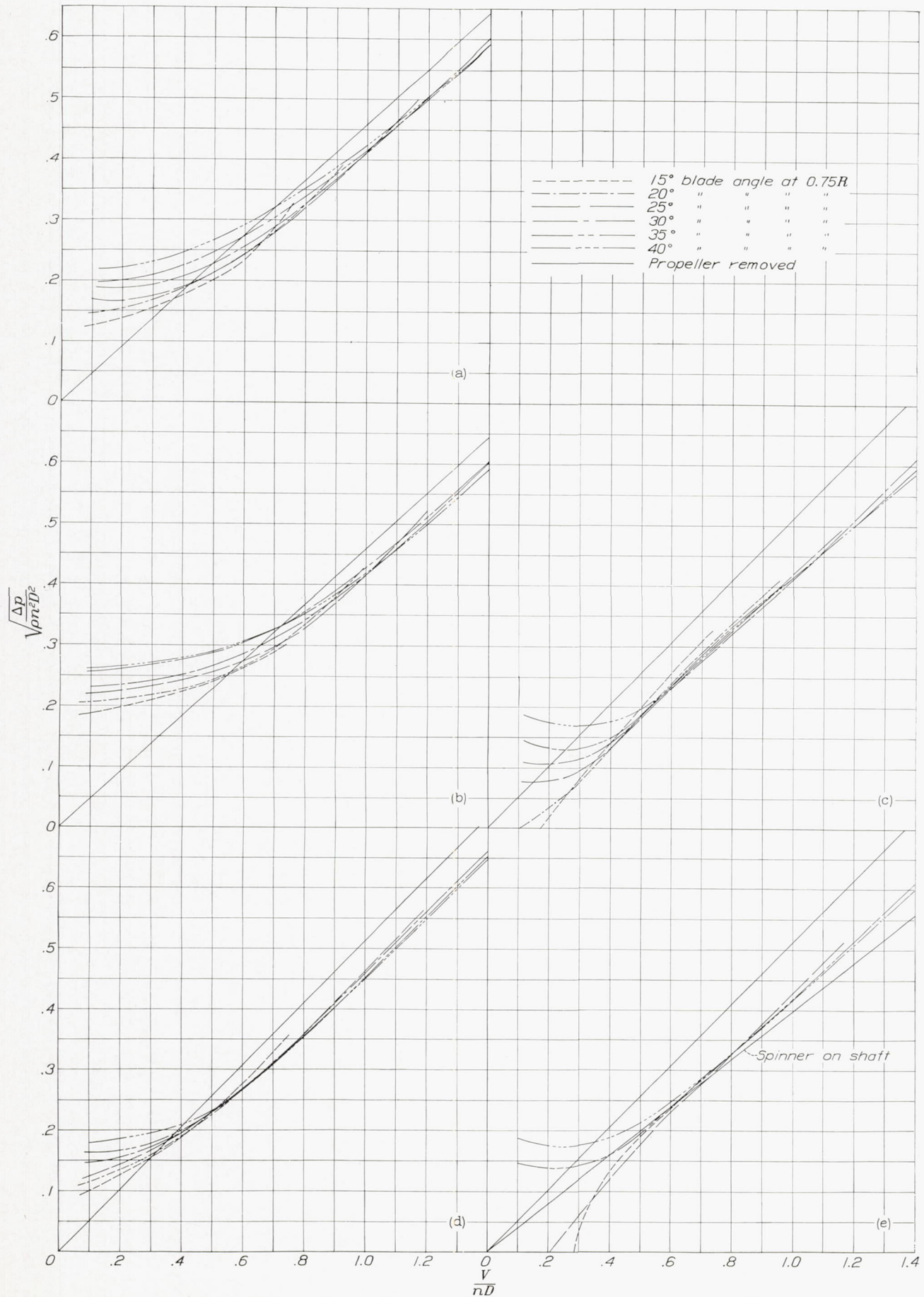


FIGURE 16.—The variation of  $\sqrt{\Delta p / \rho n^2 D^2}$  with  $V / nD$  for the various nacelle-propeller combinations tested. Cowling-flap angle,  $0^\circ$ ; the 16-in. nacelle;  $K$ , 0.085; the 12-in. nacelle;  $K$ , 0.072. (See page 17 for sublegends.)

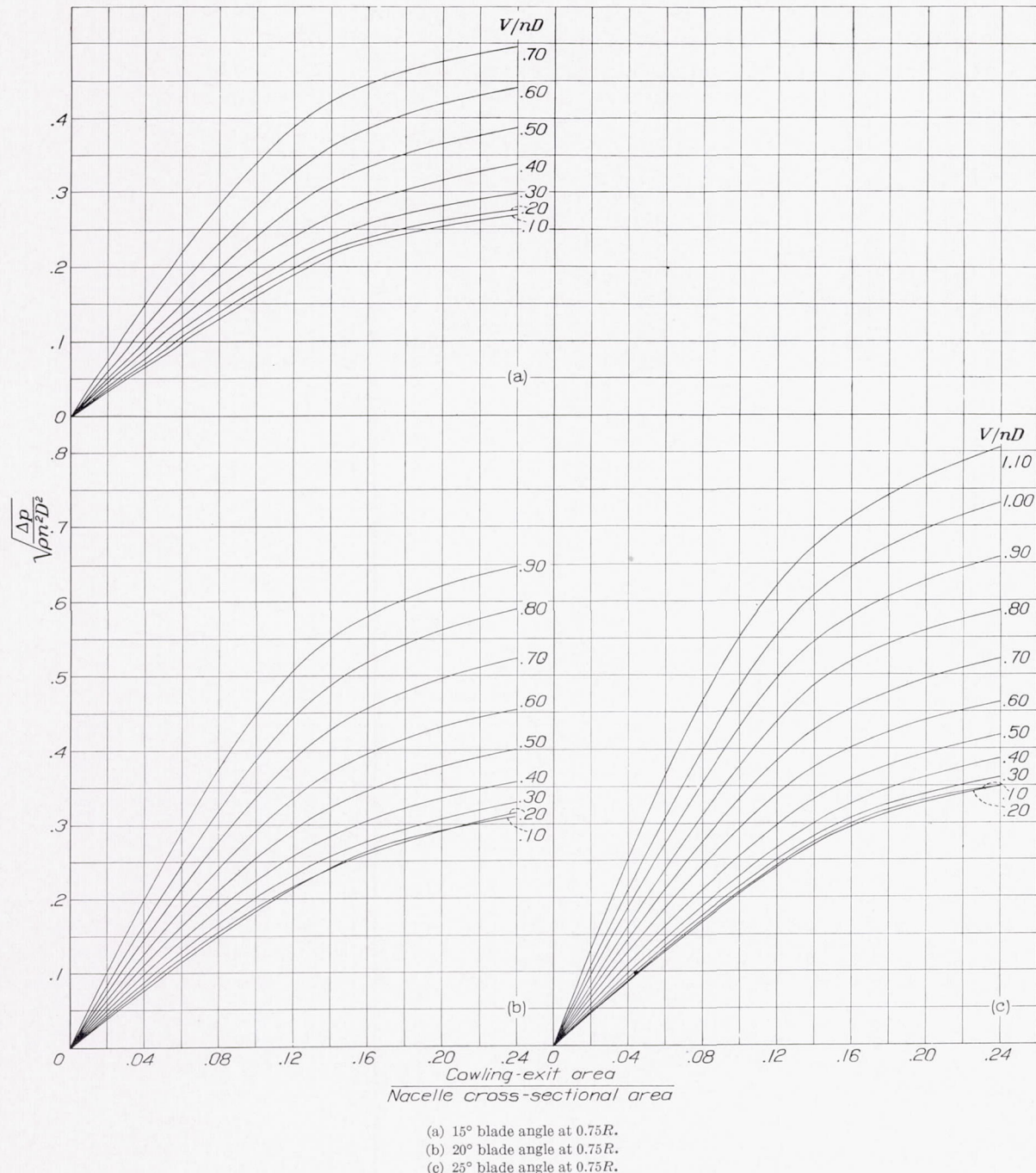


FIGURE 17.—The variation of  $\sqrt{\Delta p / \rho n^2 D^2}$  with ratio of cowling exit area to nacelle cross-sectional area. Exit area varied by cowling flaps. The 48-in. diameter propeller; the 16-in. diameter nacelle;  $K = 0.085$ .

- |  |  |   |
|--|--|---|
| (a) 48-in. propeller; 16-in. nacelle; $d/D = 0.33$ . | (c) 48-in. propeller; 12-in. nacelle; $d/D = 0.25$ . | (e) 48-in. propeller (with spinner); 12-in. nacelle; $d/D = 0.25$ . |
| (b) 36-in. propeller; 16-in. nacelle; $d/D = .44$ .  | (d) 36-in. propeller; 12-in. nacelle; $d/D = .33$ .  |   |

From the results shown in figure 18, it may appear that cowling flaps are greatly superior to the adjustable-length cowling skirt. Comparisons in figure 19 of the variation of drag with pressure drop obtained with the two systems indicate, however, that cowling flaps are slightly inferior from considerations of drag. It is to be noted that, up to a value of  $\Delta p/q$  of 0.65, the drag coefficient obtained with the variable-length skirt is

ference to show the variation of propulsive thrust with variations in that ratio.

With the arrangements tested, the effect of variation in the ratio of nacelle diameter to propeller diameter on propulsive efficiency was unimportant until the nacelle became approximately one-third of the propeller diameter but, beyond that point, the propulsive efficiency decreased rapidly with further increase in relative

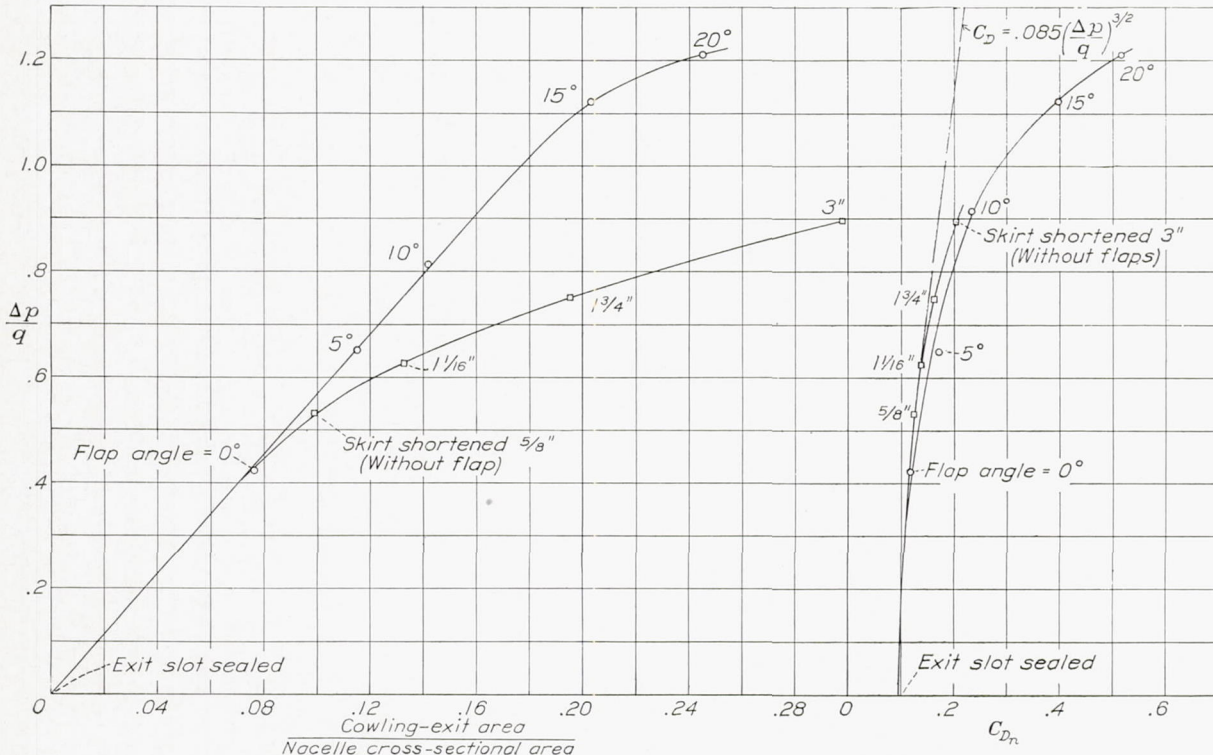


FIGURE 18.—The variation of  $\Delta p/q$  with ratio of cowling-exit area to nacelle cross-sectional area. Comparison of effect of varying exit area by cowling flaps with effect of varying exit area by reduction in cowling-skirt length. The 16-inch nacelle;  $K$ , 0.085.

the same as the theoretical cooling drag for 100 percent pump efficiency (reference 7); whereas the values of drag coefficient obtained with the cowling flaps begin to depart from the theoretical curve at a value of  $\Delta p/q$  of 0.35.

In general, the difference in drag created by the two methods is negligible in the range of values of  $\Delta p/q$  that prevail under high-speed flight conditions and is relatively small in the take-off and climbing range.

#### CONCLUDING REMARKS

These results indicate the manner in which the efficiency of a nacelle-propeller combination is dependent on the ratio of the nacelle diameter to the propeller diameter. An empirical relation has been developed from measurements of slipstream drag and body inter-

FIGURE 19.—The variation of  $\Delta p/q$  with  $C_{D_n}$ . Comparison of effect of varying exit area by cowling flaps with effect of varying exit area by reduction in cowling-skirt length. The 16-inch nacelle;  $K$ , 0.085.

body size. The highest value of net efficiency was obtained at the lowest value of the ratio of nacelle diameter to propeller diameter at which tests were made and the value decreased with increasing value of that ratio.

Tests of one nacelle-propeller combination having a ratio of nacelle diameter to propeller diameter of 0.25 showed that the presence of a spinner over the propeller hub increased the propulsive efficiency by an amount varying from 1½ to 4 percent.

Drag and cooling-air-flow measurements showed that, for a given volume of cooling-air flow, the drag of a conventional N. A. C. A. radial air-cooled engine cowling is slightly lower when fitted with an adjustable-length cowling skirt than when fitted with adjustable cowling flaps but showed that the maximum pressure

drop available with adjustable cowling flaps is about 20 percent greater than the maximum pressure available with an adjustable-length skirt.

LANGLEY MEMORIAL AERONAUTICAL LABORATORY,  
NATIONAL ADVISORY COMMITTEE FOR AERONAUTICS,  
LANGLEY FIELD, VA., April 17, 1939.

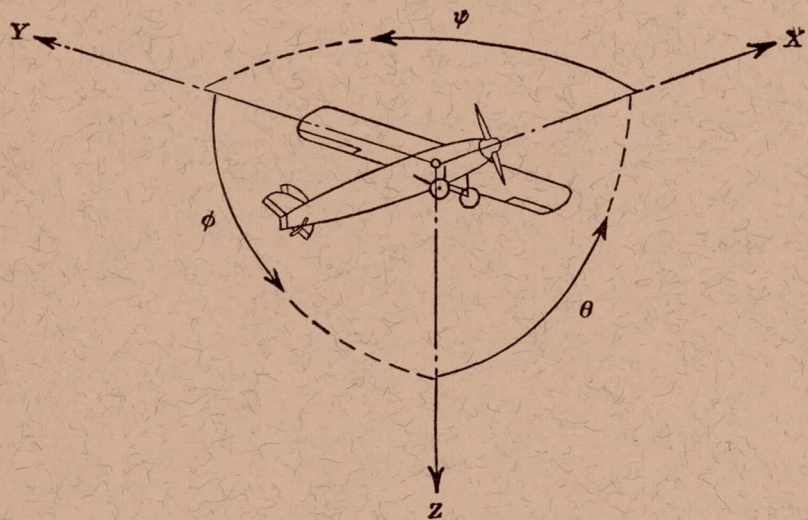
#### REFERENCES

1. Weick, Fred E.: The Effect of Reduction Gearing on Propeller-Body Interference as Shown by Full Scale Wind Tunnel Tests. T. R. No. 338, N. A. C. A., 1930.
2. Weick, Fred E.: Full-Scale Wind Tunnel Tests with a Series of Propellers of Different Diameters on a Single Fuselage. T. R. No. 339, N. A. C. A., 1930.
3. McHugh, James G.: Tests of Several Model Nacelle-Propeller Arrangements in Front of a Wing. T. R. (to be published), N. A. C. A., 1939.
4. Weick, Fred E., and Wood, Donald H.: The Twenty-Foot Propeller Research Tunnel of the National Advisory Committee for Aeronautics. T. R. No. 300, N. A. C. A., 1928.
5. Theodorsen, Theodore, Brevoort, M. J., and Stickle, George W.: Full-Scale Tests of N. A. C. A. Cowlings. T. R. No. 592, N. A. C. A., 1937.
6. Wood, Donald H.: Tests of Large Airfoils in the Propeller Research Tunnel, Including Two with Corrugated Surfaces. T. R. No. 336, N. A. C. A., 1929.
7. Wood, Donald H.: Design of Cowlings for Air-Cooled Aircraft Engines. S. A. E. Jour., vol. 41, no. 6, Dec. 1937, pp. 581-595.









Positive directions of axes and angles (forces and moments) are shown by arrows

Axis		Force (parallel to axis) symbol	Moment about axis			Angle		Velocities	
Designation	Symbol		Designation	Symbol	Positive direction	Designation	Symbol	Linear (component along axis)	Angular
Longitudinal-----	X	X	Rolling-----	L	$Y \rightarrow Z$	Roll-----	$\phi$	$u$	$p$
Lateral-----	Y	Y	Pitching-----	M	$Z \rightarrow X$	Pitch-----	$\theta$	$v$	$q$
Normal-----	Z	Z	Yawing-----	N	$X \rightarrow Y$	Yaw-----	$\psi$	$w$	$r$

Absolute coefficients of moment

$$C_l = \frac{L}{qbS}$$

(rolling)

$$C_m = \frac{M}{qcS}$$

(pitching)

$$C_n = \frac{N}{qbS}$$

(yawing)

Angle of set of control surface (relative to neutral position),  $\delta$ . (Indicate surface by proper subscript.)

#### 4. PROPELLER SYMBOLS

$D$ ,	Diameter
$p$ ,	Geometric pitch
$p/D$ ,	Pitch ratio
$V'$ ,	Inflow velocity
$V_s$ ,	Slipstream velocity
$T$ ,	Thrust, absolute coefficient $C_T = \frac{T}{\rho n^2 D^4}$
$Q$ ,	Torque, absolute coefficient $C_Q = \frac{Q}{\rho n^2 D^5}$

$P$ ,	Power, absolute coefficient $C_P = \frac{P}{\rho n^3 D^6}$
$C_s$ ,	Speed-power coefficient = $\sqrt[5]{\frac{\rho V^5}{P n^2}}$
$\eta$ ,	Efficiency
$n$ ,	Revolutions per second, r.p.s.
$\Phi$ ,	Effective helix angle = $\tan^{-1} \left( \frac{V}{2\pi r n} \right)$

#### 5. NUMERICAL RELATIONS

- 1 hp.=76.04 kg-m/s=550 ft-lb./sec.
- 1 metric horsepower=1.0132 hp.
- 1 m.p.h.=0.4470 m.p.s.
- 1 m.p.s.=2.2369 m.p.h.

- 1 lb.=0.4536 kg.
- 1 kg=2.2046 lb.
- 1 mi.=1,609.35 m=5,280 ft.
- 1 m=3.2808 ft.

